ACS APPLIED ENERGY MATERIALS

www.acsaem.org Article

A Cost-Effect Na and K Ion-Conducting Amorphous Covalent Organic Framework with High Ion Conductivity

Wonmi Lee, Haochen Li, Diprajit Biswas, Zhilin Du, Wen Ren, Lihong Zhao, Md Sariful Sheikh, Gyohun Choi, Bu Wang, Yan Yao, Eric Kazyak, and Dawei Feng*

Cite This: *ACS Appl. Energy Mater.* 2025, 8, 569−580 Read Online

ACCESS | Metrics & More | Article Recommendations | Supporting Information

ABSTRACT: Solid-state batteries utilizing sodium or potassium ions (Na- or K-ion) have emerged as promising alternatives to costly lithium-ion (Li-ion) batteries, offering a safer, more cost-effective, and sustainable solution for energy storage. Nonetheless, the practical application of these batteries is hindered by a significant challenge: the low ionic conductivity of most SEs designed for Na- or K-ion. Addressing this challenge, researchers have turned to covalent organic frameworks (COFs), a category of porous polymers characterized by their highly ordered network structures. These structures can lower the energy barrier for ion migration, thereby offering rapid pathways for ions, making COFs promising candidates as ion conductors. Sulfonated cyanurate-linked covalent organic frameworks (COFs), specifically designed for sodium or potassium ion conduction (named i-COF-1 (Na) and i-COF-1 (K)), were synthesized through a straightforward, one-step process using affordable starting materials. Remarkably, these COFs demonstrate high ionic conductivity at room temperature—1.62 × 10^{-4} S cm^{-1} for i-COF-1 (Na) and 1.15 × 10^{-4} S cm^{-1} for i-COF-1 (K)—without the need for additional salt or solvent. This enhanced performance, including low activation energies of 0.221 eV for i-COF-1 (Na) and 0.273 eV for i-COF-1 (K), is attributed to the strategic incorporation of sulfonate groups and the directional channels within the COF structure. The Na^+ and K^+ ion high conductivities, low cost, and intrinsic framework stability of i-COF-1 provide a promising SE candidate for the exploration of next generation of non-Lithium-ion secondary batteries.

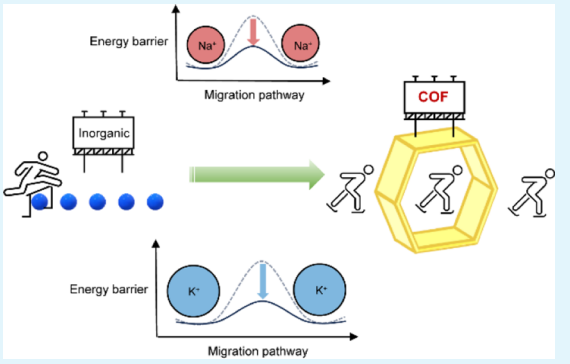

KEYWORDS: *solid electrolytes, solid-state batteries, lithium-ion batteries, covalent organic frameworks, i-COF*

INTRODUCTION

Solid electrolytes (SEs) have become a pivotal component in the advancement of solid-state batteries, offering a path to high-performance and safer energy storage solutions.[1−20] These advancements are crucial for addressing the limitations associated with liquid electrolyte-based batteries, including the risk of leakage, flammability, and restricted voltage windows. SEs boast significant benefits, such as enhanced thermal stability, nonflammability, and simplified battery design.[1] The majority of research on SEs has been concentrated on lithium-ion (Li-ion) solid-state batteries, attributed to their high ionic conductivities, which is a result of lithium's minimal ionic size among metals.[2−6] Nonetheless, given the scarcity and consequent expense of lithium resources, there is a growing consensus on the need to shift toward more cost-effective and abundantly available alternatives, such as sodium-ion (Na-ion) or potassium-ion (K-ion), for energy storage applications. Na-ion or K-ion batteries present a host of advantages over their Li-ion counterparts, not just in terms of their abundance and lower cost, but also through environmental and geopolitical benefits.[7−18] These include the potential for easier recycling, enhanced sustainability, a wide operating temperature range, and versatility across a range of applications. From large-scale energy storage systems to portable electronics and electric vehicles, Na-ion or K-ion batteries are particularly appealing in markets where cost and sustainability are critical considerations. However, the ionic conductivities of nonlithium ions, such as Na-ion or K-ion, are hindered by the high energetic barriers associated with the migration of bulkier ions within both inorganic and polymer SEs. In inorganic SEs, atoms are typically arranged in a closely packed mode, leaving limited intrinsic void space, which obstructs the diffusion of bulkier ions.[19] Meanwhile, in polymer SEs, ions are often wrapped by polymer chains, making it difficult for them to hop between coordination sites as the migrating ions increase in size.[20]

To improve the diffusivity of nonlithium ions, covalent organic frameworks (COFs) have been leveraged as SEs due to

Received: October 28, 2024
Revised: December 6, 2024
Accepted: December 9, 2024
Published: December 18, 2024

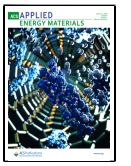

Scheme 1. Ion-Conducting Mechanisms of Inorganic, Polymer, and COF SEs[25]

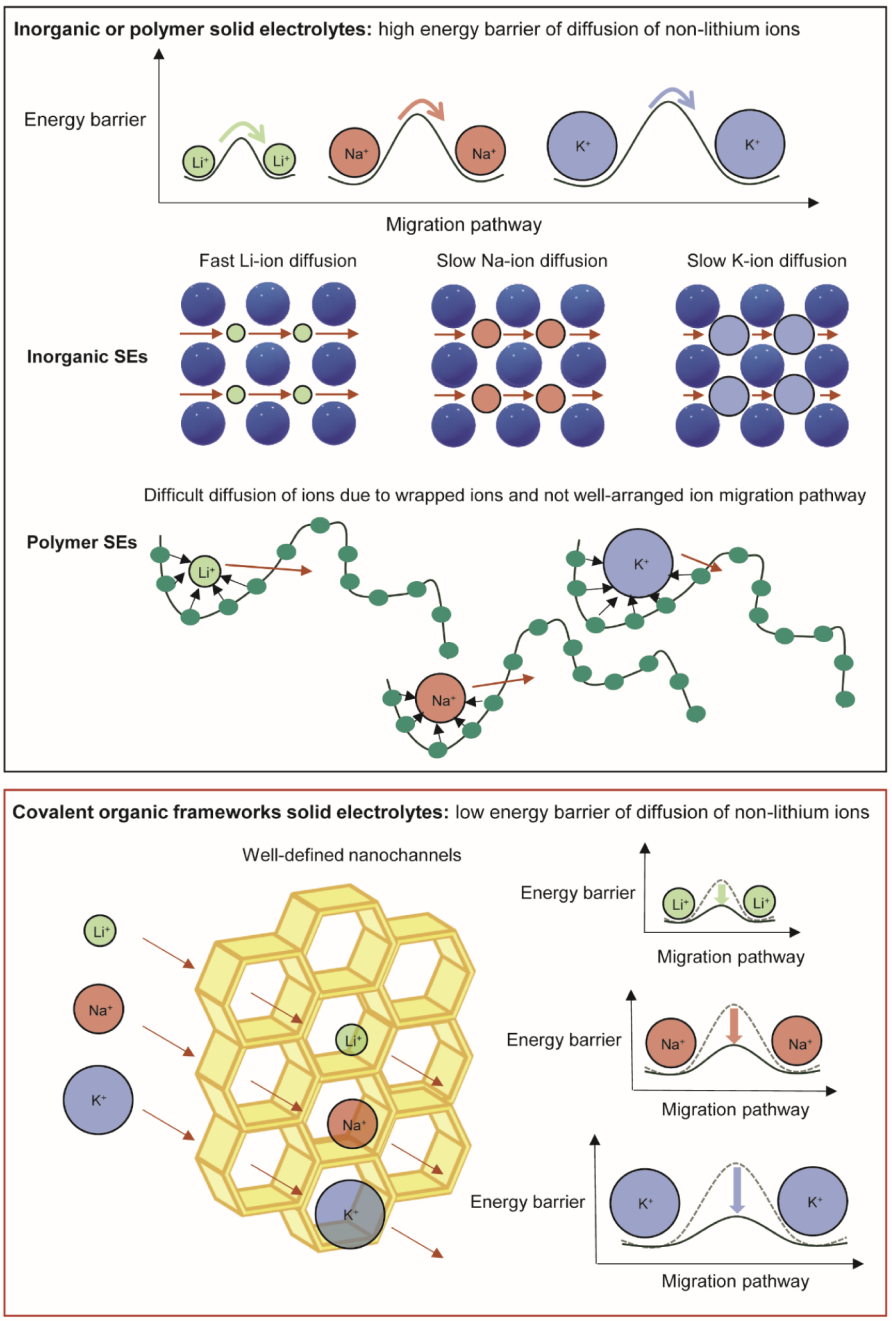

their exceptional thermal and electrochemical stability, along with notable ionic conductivity.[21−30] COFs are a class of porous polymers that exhibit two- or three-dimensional periodic structures, characterized by their micropores formed through covalent bonds between monomers rich in lightweight atoms like carbon (C), oxygen (O), nitrogen (N), and hydrogen (H). These structures can be synthesized with precise control over kinetic and thermodynamic processes, allowing for the modulation of bond formation and reversibility, resulting in highly ordered networks with specific pore sizes, shapes, and topologies.[21]

The unique features of COFs, including their long-range ordered channels, high stability, low density, and the capability for functionalization, position them as promising candidates for SEs.[22] Particularly, COFs have shown potential for achieving high ionic conductivity. Unlike inorganic and polymer SEs, which often present a high energy barrier to the migration of bulky ions due to the segmental motion of polymers or the rigid crystalline spaces of inorganic solids, COFs can significantly lower the energy barrier for ion diffusion.[23] This is attributed to their intrinsic open channels, offering ample void space for the rapid diffusion of various ions, regardless of size.[24] This mechanism of ion conduction through COFs could potentially lead to superior ionic conductivities for bulky ions (Scheme 1).[25]

Although a significant amount of research over the past decade has focused on COFs as lithium-ion conductors for Li-ion solid-state batteries,[26−32] investigations into COFs for nonlithium ions, such as Na-ion or K-ion—which are more abundant and cost-effective—have been relatively limited.

https://doi.org/10.1021/acsaem.4c02760
ACS Appl. Energy Mater. 2025, 8, 569−580

Herein, a new class of ionic COF specifically designed for sodium and potassium ion conduction—sodium sulfonated and potassium sulfonated cyanurate-linked COF, designated as i-COF-1 (Na) and i-COF-1 (K) respectively—was developed.

EXPERIMENTAL SECTION

Synthetic Methods. *Synthesis of TAZ-3P.* Cyanuric chloride, phenol, and potassium carbonate were obtained from Sigma-Aldrich, and used without further purification. 5.52 g (0.03 mol) of cyanuric chloride, 14.1 g (0.15 mol) of phenol, and 20.7 g (0.15 mol) of potassium carbonate were added to 120 mL of acetone and the solution was heated to 60 °C for 24 h. After the reaction, water was added to the solution, and it was sonicated for 10 min to remove the impurities. After that, the white product was filtered, washed with water and acetone, and vacuum-dried. A high overall yield of 90% (9.65 g) was obtained for TAZ-3P.

Synthesis of i-COF-1 (K) (Route 1). HQ-SO_3K and potassium carbonate were obtained from VWR International LLC and Thermo Scientific Chemicals, respectively. Cyanuric chloride was obtained from Sigma-Aldrich. 2.05 g (9 mmol) of HQ-SO_3K, 1.107 g (6 mmol) of cyanuric chloride and 2.49 g (18 mmol) of potassium carbonate were added to 75 mL of ethanol, and the solution was heated to 60 °C for 24 h. After the reaction, the brown product was filtered, washed with ethanol and acetone, and vacuum-dried.

Synthesis of i-COF-1 (K) (Route 2). TAZ-3P was prepared by synthesis and HQ-SO_3K and potassium carbonate were obtained from VWR International LLC and Thermo Scientific Chemicals, respectively. 2.05 g (9 mmol) of HQ-SO_3K, 1.072 g (3 mmol) of TAZ-3P and 2.49 g (18 mmol) of potassium carbonate were added to 80 mL of dimethylformamide (DMF), and the solution was heated to 150 °C for 24 h. After the reaction, the brown product was filtered, washed with DMF and acetone, and vacuum-dried. A high overall yield of 90% (4.295 g) was obtained for i-COF-1 (K).

Synthesis of i-COF-1 (Na). TAZ-3P was prepared by synthesis. HQ-SO_3Na was prepared by ion-exchange process of HQ-SO_3K, and sodium methoxide was obtained from Sigma-Aldrich. First, 1.92 g (9 mmol) of HQ-SO_3Na was added to 80 mL of dimethylformamide (DMF), and vacuum filtered to remove the impurities. After that, 1.072 g (3 mmol) of TAZ-3P and 1.0 g (18 mmol) of sodium methoxide were added into the filtrate. The solution was heated to 150 °C for 24 h. After the reaction, the brown product was filtered, washed with DMF and acetone, and vacuum-dried. A high overall yield of 81% (1.742 g) was obtained for i-COF-1 (Na).

Synthesis of COF without Sulfonate Group. TAZ-3P was prepared by synthesis and hydroquinone (HQ) and potassium carbonate were obtained from Sigma-Aldrich and Thermo Scientific Chemicals, respectively. 0.99 g (9 mmol) of HQ, 1.072 g (3 mmol) of TAZ-3P and 2.49 g (18 mmol) of potassium carbonate were added to 80 mL of dimethylformamide (DMF), and the solution was heated to 150 °C for 24 h. After the reaction, the brown product was filtered, washed with DMF and acetone, and vacuum-dried.

Characterization. *PXRD Analysis.* Powder X-ray diffraction (PXRD) patterns of the COF powder samples were obtained using a Bruker D8 Discover X-ray diffractometer. The line focused Cu X-ray tube (Cu $K_{\alpha 1}$ radiation, λ = 1.5418 Å) was set at 50 kV and 1 mA.

ATR-FTIR Analysis. To identify the formation of covalent bonds and presence of grafted sulfonate groups, the Attenuated total reflectance-Fourier transform Infrared (ATR-FT-IR) spectra of i-COF-1 (Na) and i-COF-1 (K) powders were obtained using a Thermo Scientific Nicolet iS-10 FT-IR spectrometer equipped with an Attenuated Total Reflection (ATR) element of Smart iTX AR Diamond and an OMNIC 7.3 software. The experiments run with air as the background and collected from 600 to 3000 cm^{-1}.

Solid-State CP/MAS NMR of i-COF-1 (Na) and i-COF-1 (K). To measure the solid-state 13C cross-polarization/magic angle spinning (CP/MAS) NMR spectrum of i-COF-1 (Na) and i-COF-1 (K), Bruker Avance III 500 NMR instrument with MAS III unit was used at 14 kHz spinning rate. For analyzing the solid-state 23Na of i-COF-1 (Na), the MAS with the high-power decoupling (HPDEC) method was utilized. Here, proton decoupling was used during *acquisition to suppress the dipolar interactions.*

BET Analysis. Nitrogen sorption isotherms were measured at 77 K with a Quantachrome Autosorb ASiQ automated gas sorption analyzer to identify the surface area and pore size distribution.

TGA Analysis. Thermogravimetric analysis (TGA) was conducted to identify the thermal stability of ionic COF using TA Instruments (Model TGA 550). The analysis was performed using nitrogen gas at a flow rate of 40 mL min^{-1} and the heating rate of 10 °C min^{-1}.

Electrochemical Data. *Ionic Conductivity and Activation Energy Measurements.* For ionic conductivity measurements, 100 mg of COF powder was added to a split cell (16 mm in diameter) with two stainless-steel electrodes and subjected to compression with 10 MPa for 30 min using a pressure zig to make COF powder to the pellet and sufficient contact. Electrochemical impedance spectroscopy (EIS) analysis was performed in the frequency range of 100 mHz to 1 MHz to determine the ionic conductivities at different temperatures (20, 30, 40, 50, and 60 °C). Ionic conductivity values were calculated according to the eq 1.

$$\sigma = \frac{l}{R_{total} \times A} \tag{1}$$

(Here, σ is the ionic conductivity of the sample, l is the thickness of the COF pellet, R_{total} is the total resistance, and A is the area of the COF pellet.)

Activation energy (E_a) can be calculated by the Arrhenius eq eq 2.

$$\sigma T = \sigma_0 \exp\left(-\frac{E_a}{RT}\right) \tag{2}$$

(Here, σ is the ionic conductivity of the sample, T is the temperature of conductivity measurement, R is the gas constant, and E_a is the activation energy. The slope of the Arrhenius plots changed to a lesser extent depending upon the composition of the solid electrolyte and temperature; hence the activation energy is directly proportional to the slope.)

Transference Number Measurement. The sodium- or potassium- ion transference number was derived using the Bruce-Vincent method based on chronoamperometry (CA) and EIS spectra measured before and after CA measurement of the Nali-COF-1 (Na)|Na or Kli-COF-1 (K)|K cells. Here, the freestanding roll-pressed COFs were utilized as solid electrolytes. The lithium-ion transference number can be calculated by eq 3.

https://doi.org/10.1021/acsaem.4c02760
ACS Appl. Energy Mater. 2025, 8, 569−580

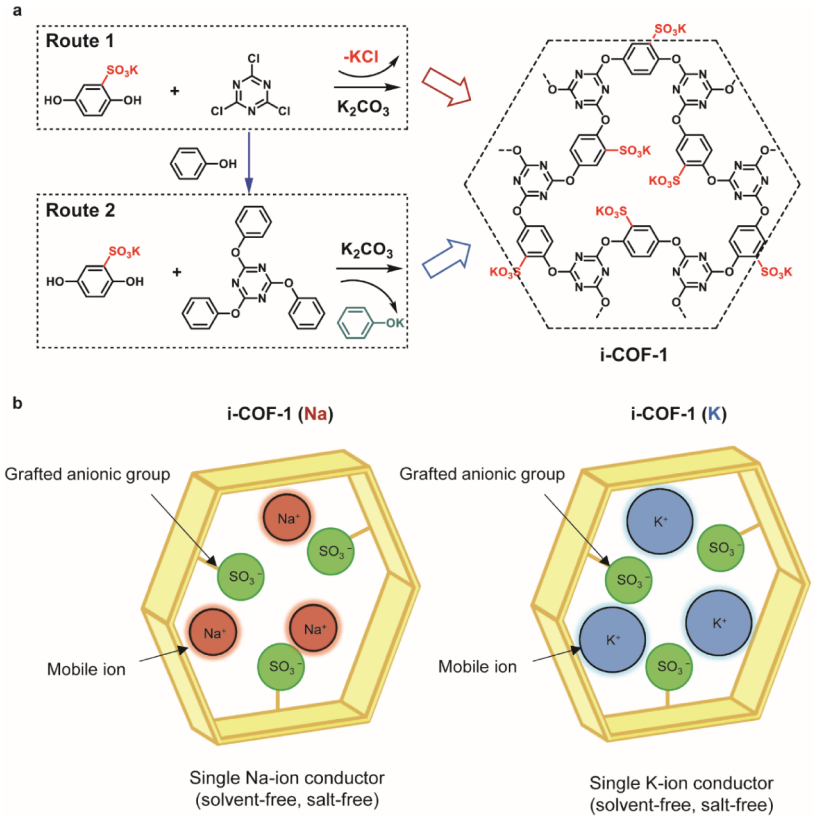

Figure 1. (a) Synthetic scheme of new design of i-COF-1 with different synthetic routes and (b) ion conducting mechanism of i-COF-1 (Na) and i-COF-1 (K).

$$t_{Li^+} = \frac{I_{ss}(\Delta V - I_0 R_0)}{I_0(\Delta V - I_{ss}R_{ss})} \quad (3)$$

(Here, t_{Li^+} is the lithium transference number, I_0 and I_{ss} are the initial and stead-state currents, ΔV is the potential applied across the cell (here, this value was 100 mV), and R_0 and R_{ss} are the initial and steady-state charge-transfer resistances SE membrane.)

Morphological Analysis. *Surface SEM/EDS Analysis.* Surface scanning electron microscopy (SEM) images of i-COF-1 (Na) and i-COF-1 (K) pellets were investigated to identify the morphology by a field-emission scanning electron microscopy (ZEISS GeminiSEM 450, Germany), using an InLens detector operating at an accelerating voltage of 5 kV. To determine the uniform distribution of atoms contained in the i-COF-1 (Na) and i-COF-1 (K), EDS measurements were conducted at 20 kV further.

In addition, SEM images of i-COF-1 (K) powders before and after ball-milling were investigated to identify the change of particle size and distribution of particles at an accelerating voltage of 3 kV. Here, the ball-milling was performed using ball-mill machine at 400 rpm for 3 h.

Ball-Milling and PEO Effect on Ionic Conductivity. *Ionic Conductivity Measurements of i-COF-1 (K) Before and After Ball-Milling.* To identify the effect of ball-milling on ionic conductivity of i-COF-1 (K), the ionic conductivity measurements were performed using 70 mg of COF powder before and after ball-milling in a split cell (16 mm in diameter) with two stainless-steel electrodes and subjected to compression with 190 MPa for 30 min. EIS analysis was performed in the frequency range of 100 mHz to 10 MHz

Ionic Conductivity Measurements of i-COF-1 (K) without and with PEO. To identify the effect of PEO on ionic conductivity of i-COF-1 (K), the ionic conductivity measurements were performed using 70 mg of COF powder without and with PEO additive in a split cell (16 mm in diameter) with two stainless-steel electrodes and subjected to compression with 190 MPa for 30 min. Here, the 20 wt % of PEO was added and both samples were ball-milled. EIS analysis was performed in the frequency range of 100 mHz to 10 MHz.

Fabrication of Freestanding i-COF-1 Solid Electrolyte and Electrochemical Measurements Using Pouch Cells. *Fabrication of Freestanding i-COF-1 Solid Electrolyte and Ionic Conductivity Measurement.* To make freestanding i-COF-1 solid electrolyte, 9:1 weight ratio of ball-milled i-COF-1 (Na) or i-COF-1 (K) with 20 wt % of PEO and PVDF binder were mixed in mortar by grinding with ethanol, and roll-pressed by roll-pressing machine at room temperature. After that, the roll-pressed sheet was dried at 60 °C onto the hot-plate overnight. The ionic conductivity was measured in a split cell (16 mm in diameter) with two stainless-steel electrodes without any pressure. EIS analysis was performed in the frequency range of 100 mHz to 10 MHz.

RESULTS AND DISCUSSION

The newly designed two-dimensional (2D) ionic COF structures presented in this study can be synthesized through a process utilizing flexible C−O−C linkages via two distinct routes (Figure 1a). Route 1 employs monomers cyanuric chloride and hydroquinone monosulfonic acid potassium salt (HQ-SO_3K) to form covalent bonds, with potassium carbonate (K_2CO_3) acting as a base. The reaction proceeds under reflux

https://doi.org/10.1021/acsaem.4c02760
ACS Appl. Energy Mater. 2025, 8, 569−580

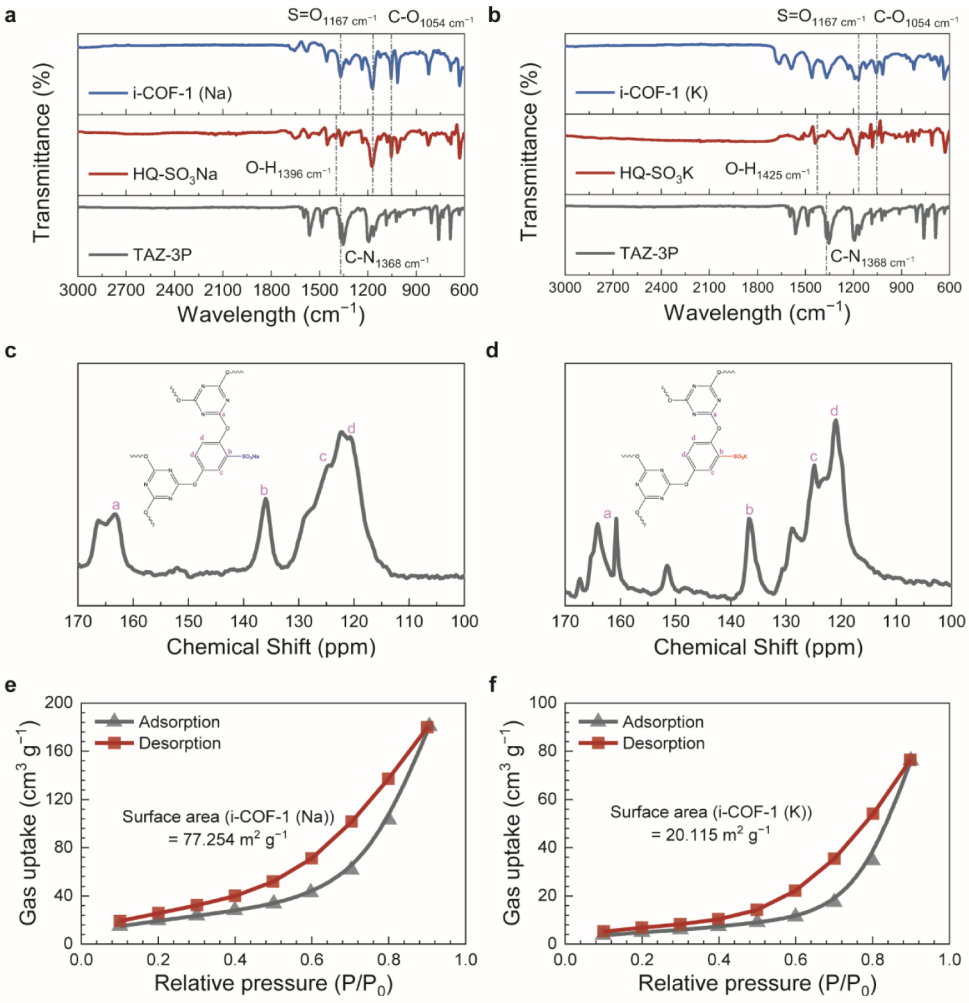

Figure 2. Structural characterizations of i-COF-1 (Na) and i-COF-1 (K). (a) and (b) ATR-FTIR of (a) i-COF-1 (Na) and (b) i-COF-1 (K). (c) and (d) Solid-state CP/MAS 13C NMR of (c) i-COF-1 (Na) and (d) i-COF-1 (K). (e) and (f) Nitrogen adsorption and desorption isotherm recorded at 77 K of (e) i-COF-1 (Na) and (f) i-COF-1 (K).

in an organic solvent for 1 day. Postreaction, the mixtures are vacuum-filtered, and the resultant solid COF powders are dried overnight at 60 °C in a vacuum oven. However, potassium chloride (KCl) is the byproduct which coprecipitates with i-COF-1 (K), affecting ion conductivity. To eliminate the interference of KCl, an alternative synthetic route was developed using TAZ-3P as a reactant to replace cyanuric chloride (Route 2), which leads to the formation of potassium phenolate, a byproduct soluble in the organic solvent used during synthesis. Therefore, only i-COF-1 (K) crashed out as pure product. Powder X-ray diffraction (PXRD) analysis confirmed the presence of KCl in i-COF-1(K) produced by Route 1, while i-COF-1 (K) synthesized by Route 2 exhibited its characteristic peaks (Figure S1). Similarly, i-COF-1 (Na) can be synthesized by using hydroquinone monosulfonic acid sodium salt (HQ-SO_3Na) and sodium methoxide ($NaOCH_3$) instead of HQ-SO_3K and K_2CO_3, respectively, via Route 2. This synthesis method is both straightforward and cost-efficient, relying on readily available starting materials. Furthermore, PXRD analysis indicated that i-COF-1 has an amorphous structure, with no peaks corresponding to monomers (Figure S2).

The integration of $-SO_3^-$ groups and directional channels within the COF structure enhances the diffusivity of Na-ion or K-ion through a hopping mechanism, ensuring efficient pathways for rapid ion transport (Figure 1b). Furthermore, the presence of anchored sulfonate groups acts as carriers for Na- or K-ion, resulting in a salt-free, solvent-free, and uniquely efficient single Na-ion or K-ion conducting SE. This innovative approach paves the way for the development of more effective and sustainable energy storage technologies.

The ionic COF powders prepared were analyzed using Fourier transform infrared (FT-IR) spectroscopy, revealing distinct features in their spectra (Figure 2a,b). The FT-IR spectrum of i-COF-1 (Na) displayed characteristic peak (C−N) at 1368 cm^{-1}, mirroring those found in TAZ-3P, which confirmed the presence of a triazine core. Notably, a peak at 1396 cm^{-1} observed in HQ-SO_3Na was absent in i-COF-1 (Na), indicating that the −OH group was utilized as a building block to form the covalent bond, which was observed at 1054 cm^{-1} (C−O−C group). Additionally, the emergence of a peak at 1167 cm^{-1} in i-COF-1 (Na) and HQ-SO_3Na corresponds to the $-SO_3$Na group,[31] indicating successful integration of the potassium sulfonate group within the COF structure. Similar alterations in IR transmittance were also observed for i-COF-1 (K), indicating a parallel integration process of the potassium sulfonate group.

https://doi.org/10.1021/acsaem.4c02760
ACS Appl. Energy Mater. 2025, 8, 569−580

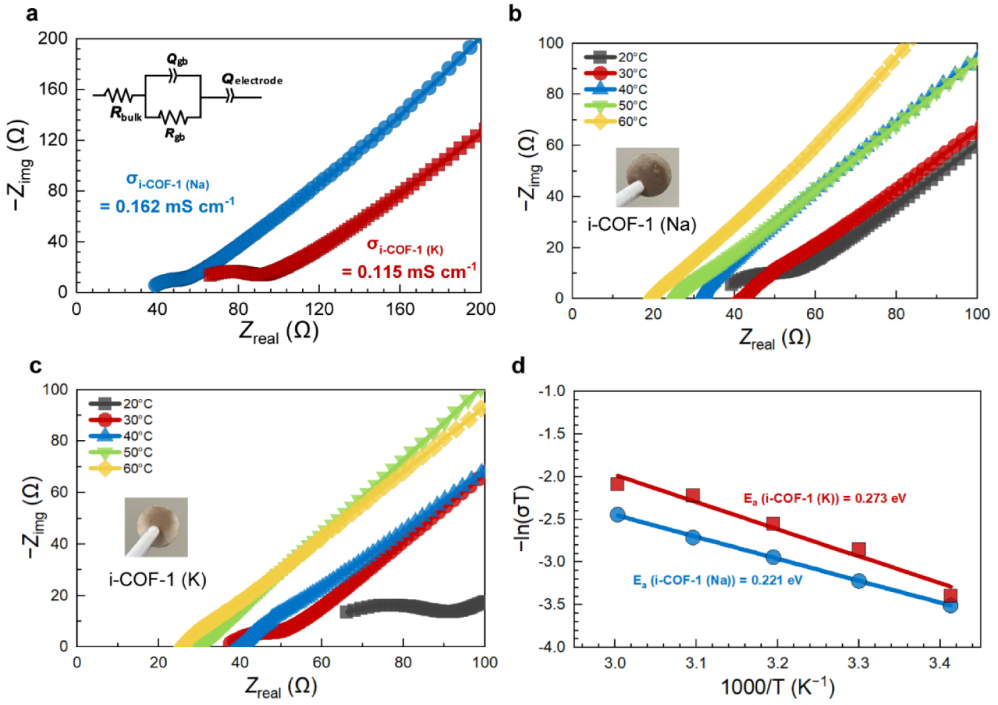

Figure 3. Ionic conducting properties of i-COF-1 (Na) and i-COF-1 (K). (a) Ionic conductivity at room temperature. (b) and (c) EIS plots at different temperatures of (b) i-COF-1 (Na) and (c) i-COF-1 (K). (Inset pictures are i-COF-1 pellets prepared under pressure of 190 MPa). (d) Activation energy of i-COF-1 (Na) and i-COF-1 (K).

Solid-state CP/MAS 13C NMR of i-COF-1 (Na) and i-COF-1 (K) was analyzed to investigate the chemical environment of each C atom in COF materials (Figure 2c,d). The peak at 163 ppm is related to the C signal in the triazine ring, whereas the two peaks at 124 and 122 ppm are observed due to the presence of benzene ring-containing C atoms. Another peak at 136 ppm is attributed to the sulfonate group adjacent to the C atom. Furthermore, solid-state direct 23Na NMR of i-COF-1 (Na) was analyzed to identify the chemical environment of sodium atom, and the peaks near the −6 and 1 ppm were observed, which are related to the sodium atom attached to the O atom in the sulfonate groups (Figure S3).

The surface area and pore size distribution of i-COF-1 (Na) and i-COF-1 (K) were determined through Nitrogen gas adsorption analysis at 77 K (Figures 2e,f and S4). The analysis revealed surface areas of 77.254 m^2 g^{-1} for i-COF-1 (Na) and 20.115 m^2 g^{-1} for i-COF-1 (K) (Figure 2e,f). Additionally, the pore volumes were measured at 0.259 cc g^{-1} for i-COF-1 (Na) and 0.105 cc g^{-1} for i-COF-1 (K) (Figure S4). The pore radius of both i-COF-1 (Na) and i-COF-1 (K) (2.48 and 2.59 nm, respectively) are larger than the ionic radius of sodium and potassium ions (0.095 and 0.133 nm, respectively), leading to high ionic conductivity of bulky ions. These values are considerably lower than those typically observed for COFs, likely due to the relatively small pore sizes within the i-COF-1 framework and the presence of a substantial amount of sulfonate and counter alkali ions (i.e., Na^+ and K^+).

Thermogravimetric analysis (TGA) demonstrated the thermal stability of i-COF-1 (Na) and i-COF-1 (K), with no structural decomposition observed up to 400 °C (Figure S5). The slight weight loss observed before 400 °C may be due to the evaporation of trapped solvent or the decomposition of residual monomers. Furthermore, at 700 °C, i-COF-1 (Na) and i-COF-1 (K) retained over 60 and 70 wt % of their original mass, respectively. This remarkable thermal stability underscores the potential of both i-COF-1 (Na) and i-COF-1 (K) for applications under extreme conditions, including high temperatures.

The ionic conducting properties of i-COF-1 (Na) and i-COF-1 (K) were evaluated through electrochemical measurements (Figure 3). Initially, the ionic conductivity at room temperature (20 °C) was determined using electrochemical impedance spectroscopy (EIS) (Figure 3a). For assessing the ionic conductivity of the COF materials, the COF powders were placed between stainless steel electrodes in a split cell configuration, acting as a blocking cell. These were then compressed under a pressure of 190 MPa for 30 min to form a uniform COF pellet (Figure S6).

The EIS analysis incorporated an equivalent circuit model to interpret the impedance data, as illustrated in the inset of Figure 3a. This model includes components for the bulk resistance (R_{bulk}) and the grain boundary resistance (R_{gb}), with the total resistance (R_{total}) being the sum of these two resistances.[32] The fitting of the EIS data utilizes an equivalent circuit composed of R_{bulk}, R_{gb}, along with constant phase elements Q_{gb} and $Q_{electrode}$, where "R" denotes resistance and "Q" represents a constant phase element indicative of nonideal capacitive behavior. The bulk and grain boundary resistances are inferred from the x-intercept and the diameter of the semicircle in the low-frequency region of the impedance plot, respectively. Consequently, R_{total} is calculated as the sum of R_{bulk} and R_{gb}. The slope in the low-frequency region is associated with mass transfer resistance. Both i-COF-1 (Na) and i-COF-1 (K) exhibited slopes greater than 1 but less than 2, indicating anomalous diffusion caused by heterogeneous ion transport pathways within the SEs. This behavior is likely due to the influence of grain boundaries or interfacial factors.[33,34]

https://doi.org/10.1021/acsaem.4c02760
ACS Appl. Energy Mater. 2025, 8, 569−580

Table 1. Ion Conductivity Comparison of Newly Developed Ionic COF with Other COFs or MOFs

Solid electrolyte	Conducting ion	Additional solvent or salt	$\sigma_{(RT)}$ S cm^{-1}	temperature	Reference
NaOOC−COF	Na-ion	liquid electrolyte (10.0 μL, 1.0 M) of $NaPF_6$ (in propylene carbonate, PC)	2.68×10^{-4}	RT	35
TPDBD-CNa-QSSE	Na-ion	9 wt.% solvents (PC) with 5% FEC	1.30×10^{-4}	RT	36
MIL-121/Na	Na-ion	50 wt % of 1 M $NaClO_4$ in PC	1.0×10^{-4}	RT	37
UIOSNa	Na-ion		3.6×10^{-4}	RT	38
PHGE-Na	Na-ion		3.48×10^{-3}	RT	39
COF-1-Na	Na-ion	98% relative humidity	2.5×10^{-2}	313 K	40
MOF-808-SO_3K	K-ion	20 μL of anhydrous PC	3.1×10^{-5}	303 K	41
TpPa-SO_3Li	Li-ion		2.7×10^{-4}	RT	42
PEO-n-UIO	Li-ion	40% UIO/Li-IL	1.3×10^{-4}	303 K	43
dCOF-ImTFSI-60	Li-ion		2.79×10^{-3}	373 K	44
CF_3−Li-Im-COF	Li-ion	n-BuLi, 20 wt %PC	7.20×10^{-3}	RT	45
LE@ACOF	Li-ion	Li-ion	3.70×10^{-3}	RT	46
i-COF-1 (Na)	**Na-ion**	-	1.62×10^{-4}		**This work**
i-COF-1 (K)	**K-ion**	-	1.15×10^{-4}		**This work**

Scheme 2. Possible Ion Conducting Mechanism of i-COF-1; (a) Ion Hopping Scheme within One Pore; (b) Ion Hopping Scheme from One Pore to Another Pore (Through-Plane); (c) Ion Hopping Scheme from One Pore to Another Pore (In-Plane)

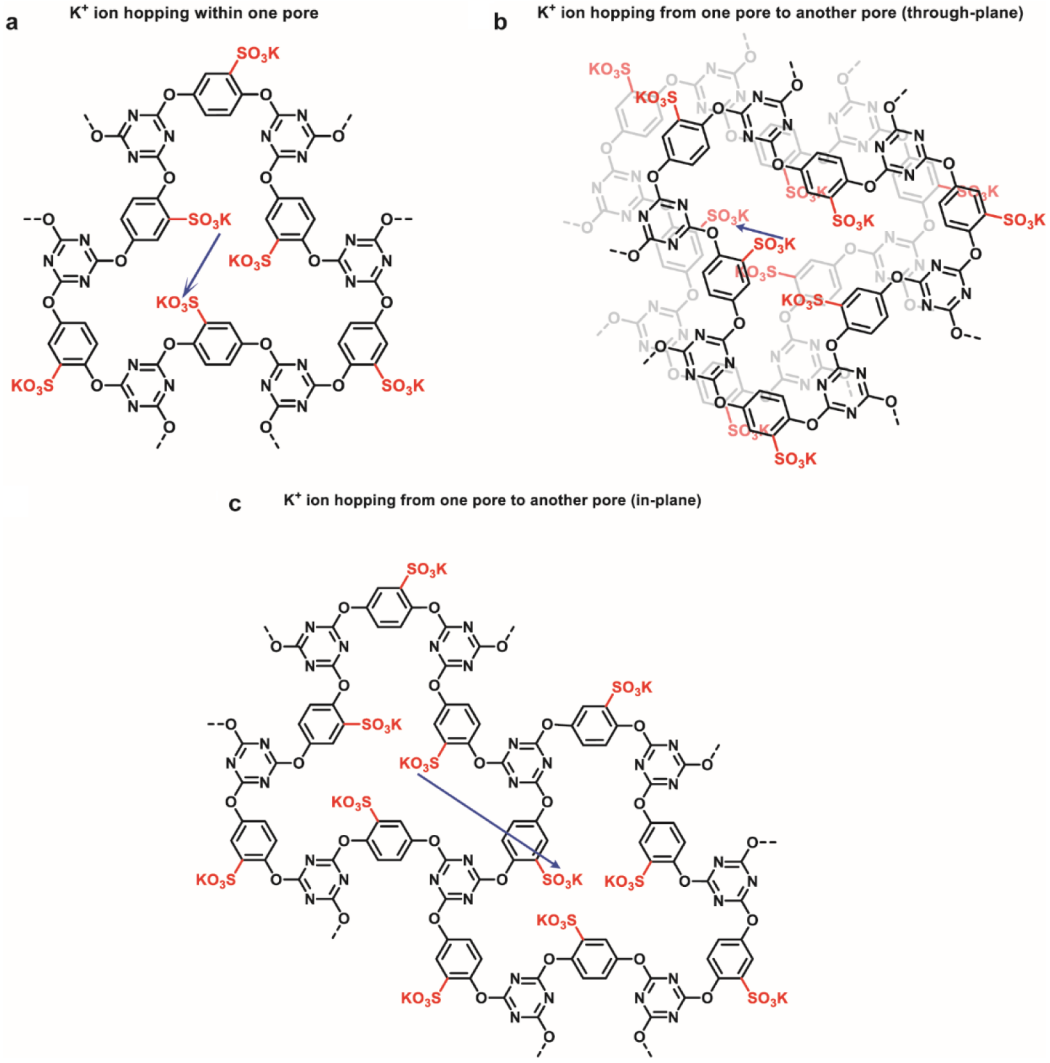

The ionic conductivities of i-COF-1 (Na) and i-COF-1 (K) at room temperature were determined to be 1.62×10^{-4} and 1.15×10^{-4} S cm^{-1}, respectively. These values, indicative of high ionic conductivity, underscore the unique and superior ionic mechanism facilitated by the ionic COF structure, which achieves significant conductivity despite the generally slow diffusivity of Na- or K-ion. These conductivity figures are comparable to, or exceed, those reported for other COFs or

https://doi.org/10.1021/acsaem.4c02760
ACS Appl. Energy Mater. 2025, 8, 569−580

metal−organic frameworks (MOFs), highlighting the potential of i-COF-1 materials in ionic conduction applications (Table 1).[35−46] Unlike many other COFs or MOFs that exhibit high ionic conductivity typically through the addition of salts or solvents, it is notable that our i-COF-1 demonstrates exceptional ionic conductivities without the need for such additions. This distinct characteristic underscores the intrinsic ionic conduction capabilities of i-COF-1, facilitated by its unique structural composition.

Further investigation into the ion-hopping activation energy (E_a) within i-COF-1 (Na) and i-COF-1 (K) was conducted through electrochemical EIS measurements of COF pellets at varying temperatures (20, 30, 40, 50, and 60 °C) (Figures 3b-d, S7). The results, interpreted using the previously mentioned equivalent circuit model, reveal a progressive increase in ionic conductivity with temperature. Specifically, the ionic conductivities of i-COF-1 (Na) ranged from 1.62×10^{-4} S cm^{-1} at 20 °C to 4.70×10^{-4} S cm^{-1} at 60 °C. Similarly, i-COF-1 (K) exhibited conductivities from 1.15×10^{-4} S cm^{-1} at 20 °C to 3.73×10^{-4} S cm^{-1} at 60 °C. The activation energies calculated for i-COF-1 (Na) and i-COF-1 (K) were 0.221 and 0.273 eV, respectively. These relatively low E_a values highlight the efficient ion migration within i-COF-1, facilitated by the directional porous channels and the strategically integrated sulfonate groups. Charged groups, such as sulfonate or carboxylic groups, can significantly promote ion conductivity. For example, Sun et al. developed a sodium ion-conducting carboxylated COF SE (NaOOC−COF) and investigated the ion-conducting pathway using DFT calculations.[35] Based on these calculations, the conjugated framework could promote the dissociation between carboxylic anions and Na cations by weakening the electrostatic interaction between them. Similarly, Lee et al. introduced a new lithium-ion-conducting sulfonated COF SE (TpPa-SO_3Li) and also revealed the ion-conducting mechanism through DFT calculations.[42] The O atoms in the sulfonate groups enhance the thermodynamic stability of Li-ion intermediates in the axial pathway, leading to high ionic conductivity.

In our study, the possible ion-conducting mechanism is shown in Scheme 2. Ions can be conducted via a hopping mechanism within a single pore or from one pore to another, either through-plane or in-plane. Here, the amorphous i-COFs offer shorter ion-hopping distances due to their random stacking, making them an attractive option for use as SEs. Additionally, amorphous i-COFs are easier to synthesize compared to their crystalline counterparts and demonstrate high ionic conductivity, further supporting their suitability for this application. Furthermore, the sulfonate groups can act as hopping sites. To prove the effect of sulfonate groups in COF on the ion conductivity, we synthesized a COF without sulfonate groups and measured the ionic conductivity using the same EIS test method (Figure S8). The resistance was too high, indicating that the ionic conductivity was too low due to the absence of sulfonate groups. The outstanding ion-conducting performance of i-COF-1 is attributed to its high density of mobile charge carriers, coupled with the intrinsic porous structure. This configuration ensures a greater number of mobile ionic species and shorter hopping distances for ion transport, setting a new benchmark for the design and development of advanced SEs in energy storage technologies.

In addition, the ionic conductivity of i-COF-1 (K) was measured at various thicknesses to observe the thickness effect under 190 MPa (Figure S9). The thickness was controlled by using different weights of COF powders. The ionic conductivities at 191, 272, and 355 μm (70, 100, and 130 mg) were 1.15×10^{-4}, 8.77×10^{-5}, and 8.37×10^{-5} S cm^{-1}, respectively (Figure S9a and c). However, the ionic conductivity was too low when the thickness was 518 μm (160 mg), possibly due to insufficient interfacial contact between particles (Figure S9b).

Similarly, various pressures were applied to observe the pressure effect on ionic conductivity when measuring the EIS using 100 mg of i-COF-1 (K) (Figure S10). The ionic conductivity under 10 MPa was too low due to insufficient interfacial contact between particles (Figure S10a). In contrast, the ionic conductivities under 70, 130, and 190 MPa were 2.03×10^{-5}, 4.25×10^{-5}, and 8.77×10^{-5} S cm^{-1}, respectively (Figure S10b and c).

Scanning electron microscopy coupled with energy dispersive X-ray spectroscopy (SEM/EDS) analyses of i-COF-1 (Na) and i-COF-1 (K) pellets were conducted to examine the morphology of the ionic COFs and ensure the uniform distribution of their constituent elements (Figures 4a−l and S11). The SEM images highlighted the uniform packing of COF powders within the pellets, indicating successful compaction and structural integrity. Furthermore, EDS analysis provided a detailed elemental distribution within the pellets, confirming the presence and uniform distribution of C, N, O, sulfur (S), and sodium (Na) in the i-COF-1 (Na) pellet. Similarly, for the i-COF-1 (K) pellet, elements including C, N, O, S, and potassium (K) were uniformly distributed. These findings underscore that the sulfonate groups, −SO_3Na and −SO_3K, were effectively grafted into the COF structures, and the pellets were uniformly prepared through a pressing method

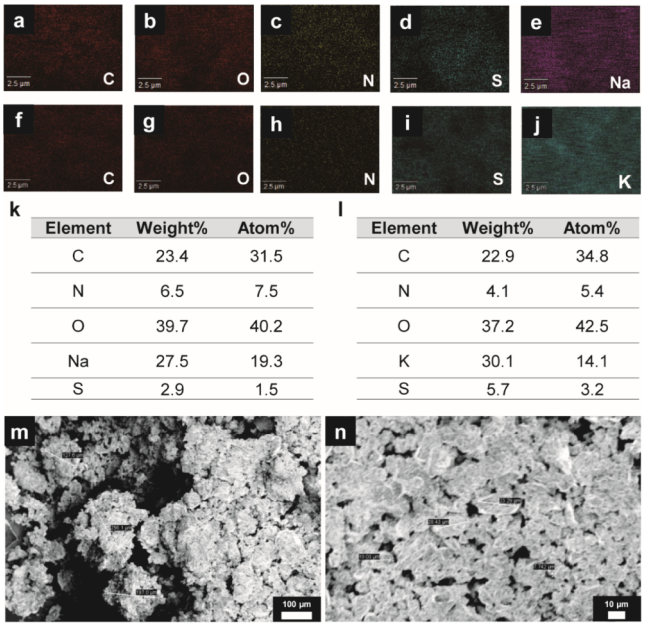

Element	Weight%	Atom%
C	23.4	31.5
N	6.5	7.5
O	39.7	40.2
Na	27.5	19.3
S	2.9	1.5

Element	Weight%	Atom%
C	22.9	34.8
N	4.1	5.4
O	37.2	42.5
K	30.1	14.1
S	5.7	3.2

Figure 4. EDS mapping of i-COF-1 (Na) and i-COF-1 (K) and morphological images of i-COF-1 (K) powders before and after ball-milling. (a)−(e) EDS mapping of i-COF-1 (Na) (a: C atom, b: O atom, c: N atom, d: S atom, e: Na atom).(f)−(j) EDS mapping of i-COF-1 (K) (f: C atom, g: O atom, h: N atom, i: S atom, j: K atom).Atomic ratio of each element in EDS mapping of (k) i-COF-1 (Na) and (l) i-COF-1 (K). SEM image with particle size of i-COF-1 (K) powder (m) before and (n) after ball-milling.

https://doi.org/10.1021/acsaem.4c02760
ACS Appl. Energy Mater. 2025, 8, 569−580

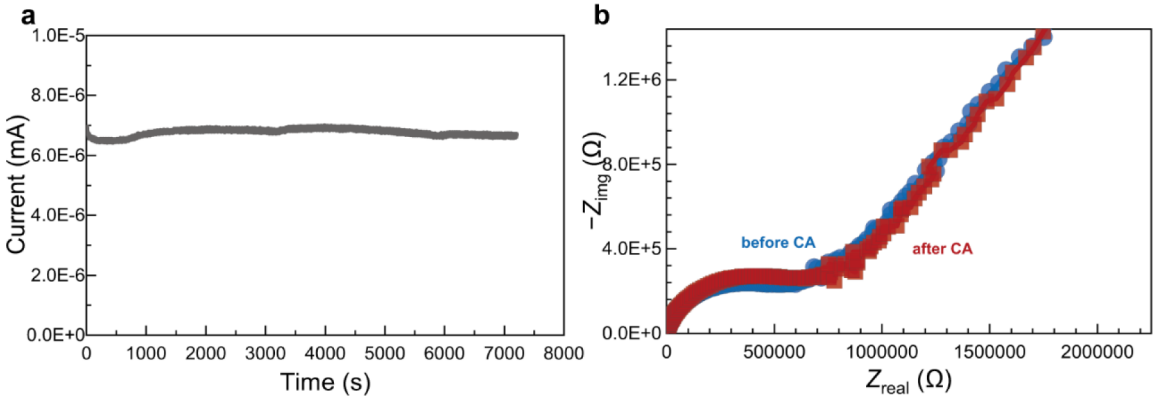

Figure 5. Transference number measurement of i-COF-1 (Na). (a) CA curve and (b) EIS plots before and after CA measurement of i-COF-1 (Na).

at a pressure of 190 MPa. This uniform elemental distribution and the integrity of the COF structure are crucial for ensuring consistent ionic conductivity and the overall performance of the COFs as SEs. The successful grafting of sulfonate groups and the demonstrated uniformity in pellet preparation highlight the potential of i-COF-1 materials in advanced energy storage applications, offering a reliable and efficient medium for ion transport.

Furthermore, SEM images of i-COF-1 (K) before and after ball-milling were obtained to observe the effect on particle size and distribution (Figure 4m,n). The particle size of i-COF-1 (K) powder after ball-milling was smaller and exhibited a more uniform distribution compared to that before ball-milling.

To investigate the effect of ball-milling on ionic conductivity, the ionic conductivities of 70 mg of i-COF-1 (K) powders before and after ball-milling were measured (Figure S12). The ball-milled i-COF-1 (K) exhibited an enhanced ionic conductivity of 1.31×10^{-4} S cm^{-1}, compared to the pristine i-COF-1 (K), which showed a conductivity of 1.15×10^{-4} S cm^{-1}. Furthermore, the effect of the PEO additive on ionic conductivity was examined. PEO can improve the interfacial contact between COF particles and act as a binder, which is helpful for preparing a freestanding SE. As shown in Figure S13, the ionic conductivity of i-COF-1 (K) with the PEO additive (1.67×10^{-4} S cm^{-1}) was slightly lower than that of i-COF-1 (K) without the PEO additive ($1.31 \times \times 10^{-3}$ S cm^{-1}). However, the addition of a PVDF binder, along with the PEO, helps in making a freestanding SE, and the ionic conductivity remains high enough (8.98×10^{-4} S cm^{-1}) (Figure S14).

The transference number was obtained using the Bruce-Vincent method with small pouch cells configured as Nali-COF-1 (Na)|Na (Figure 5). Chronoamperometry (CA) and electrochemical impedance spectroscopy (EIS) were performed before and after CA to calculate the transference number. The sodium-ion transference number for i-COF-1 (Na) is 0.9, demonstrating the single ion conductivity of i-COF-1. We also noticed there is a significant increase in the resistance (Figure 5b) during the symmetric cell measurement, which we suspect is due to the resistive interface formation between i-COF-1 and Na metal. Additionally, the straight line observed in the low-frequency region is attributed to mass transport resistance. The slope of approximately 1.2 indicates anomalous diffusion, which stems from structural complexities such as grain boundaries, interfacial polarization, and defects within the SE or at the interface between the SE and the Na metal electrode.

The comprehensive characterizations and electrochemical measurements presented affirm that i-COF-1 (Na) and i-COF-1 (K) possess exceptional attributes, facilitating high ionic conductivity for the cost-effective and abundant Na and K ions. This breakthrough underscores the potential of these newly developed ionic COFs as economically viable materials, leveraging low-cost starting materials that are significantly more affordable than most inorganic SEs. While some inorganic SEs may also utilize inexpensive materials, their susceptibility to air limits their practical application due to stability concerns.[47] In contrast, COFs demonstrate remarkable air stability, positioning them as promising SEs in terms of both cost-effectiveness and durability.[48] The synthesis of TAZ-3P, a critical monomer for constructing the ionic COF, employs affordable raw materials such as cyanuric chloride, phenol, and potassium carbonate, which contributes to the low synthesis cost of TAZ-3P. Similarly, HQ-SO_3Na, another monomer used in the synthesis of i-COF-1 (Na), can be produced using inexpensive starting materials, including HQ-SO_3K and sodium tetrafluoroborate ($NaBF_4$). Consequently, the production costs for i-COF-1 (Na) remain low, utilizing cost-effective precursors such as TAZ-3P, HQ-SO_3Na, and sodium methoxide. The synthesis of i-COF-1 (K) also benefits from the use of low-cost materials, including TAZ-3P, HQ-SO_3K, and potassium carbonate. Given that SEs constitute a significant portion of the overall costs in energy storage devices, the introduction of these novel ionic COFs could markedly reduce the expense associated with such devices. This advantage, combined with their superior performance and stability, highlights the potential of i-COF-1 materials in advancing the development of more affordable and sustainable energy storage solutions.

Additionally, i-COF-1 (Na) and i-COF-1 (K) exhibited high solubility in water (1g/1 mL), which can be beneficial for easy recyclability (Figure S15). High solubility in water facilitates the recycling of materials by simplifying separation and purification processes, potentially making them less energy-intensive.

CONCLUSIONS

This research introduces a groundbreaking class of single-ion conductors: sulfonated ionic COF containing Na- or K- ion within their framework structures (i-COF-1 (Na) and i-COF-1 (K)). These materials are designed to be solvent-free and salt-free, positioning them as cost-effective alternatives for energy storage applications. A comparative analysis with other SEs,

https://doi.org/10.1021/acsaem.4c02760
ACS Appl. Energy Mater. 2025, 8, 569−580

Table 2. Ion Conducting Properties Comparison of Newly Developed ionic COF with Other SEs

Solid electrolyte	Conducting ion	$\sigma_{(RT)}$ S cm^{-1}	temperature	Reference
$Na_{3.4}Sc_2Si_{0.4}P_{2.6}O_{12}$	Na-ion	6.9×10^{-4}	RT	[R49
$Na_{3.4}Sc_{0.4}Zr_{1.6}Si_2PO_{12}$	Na-ion	1.9×10^{-3}	RT	[R50
$Na_3Zr_2(SiO_4)_2PO_4$ (NZSP)	Na-ion	9.66×10^{-4}	RT	[R51
$Na_{3.4}Zr_2Si_{2.4}P_{0.6}O_{12}$ (NZSP) with 2.5 mol % $Na_3LaP_2O_8$ (NLP)	Na-ion	7.1×10^{-3}	RT	[R52
Ca^{2+} doped $Na_{2.7}Ca_{0.15}Zr_2Si_2PO_4$	Na-ion	1.53×10^{-4}	RT	[R53
$Na_{3.125}Zr_{1.75}Sc_{0.125}Ge_{0.125}Si_2PO_{12}$	Na-ion	4.64×10^{-3}	RT	[R54
$Na_{3.3}La_{0.3}Zr_{1.7}Si_2PO_{12}$ (NLZSP0.3)	Na-ion	1.34×10^{-3}	RT	[R55
Na-β''-Al_2O_3	Na-ion	2.1×10^{-3}	RT	[R56
Sodium β-alumina (SBA) with 15 wt % $NaPF_6$	Na-ion	5.91×10^{-4}	RT	[R57
Na−LaCeZrHfTa−Cl	Na-ion	8.8×10^{-4}	RT	[R58
K−LaCeZrHfTa−Cl	K-ion	1.32×10^{-6}	328 K	[R58
$Li_{3.2}Ge_{0.2}P_{0.8}O_4$	Li-ion	5.3×10^{-4}	300 K	[R59
$Li_{10}Ge(P_{0.95}Sb_{0.05})_2S_{12}$	Li-ion	1.71×10^{-2}	RT	[R60
$Li_{2.5}Zr_{0.5}Y_{0.5}Cl_6$	Li-ion	1.4×10^{-3}	RT	[R61
$Li_{10.5}Sn_{0.3}Si_{1.2}P_{1.5}S_{12}$	Li-ion	8.2×10^{-3}	300 K	[R62
$Li_{10}GeP_2S_{12}$	Li-ion	2.7×10^{-2}	RT	[R63
i-COF-1 (Na)	**Na-ion**	1.62×10^{-4}		**This work**
i-COF-1 (K)	**K-ion**	1.15×10^{-4}		**This work**

including sulfide, halide, and beta-alumina SEs, reveals that the Na-ion conductivity of these ionic COFs is comparable or slightly lower than that of other high-performance SEs (Table 2).[49−63] Despite this, the ionic COFs distinguish themselves through their superior stability and cost-effectiveness, addressing the common challenges of high processing temperatures, expensive materials, and air sensitivity associated with inorganic or halide SEs that exhibit high Na-ion conductivity. Notably, the K-ion conductivity of the developed ionic COFs significantly surpasses that of other SEs, showcasing their exceptional ionic conducting properties. This performance is attributed to the reduced energy barrier for ion migration, facilitated by a well-organized porous structure and the incorporation of sulfonate anionic groups. This advancement in ion conductivity positions ionic COFs as viable alternatives to expensive Li-ion batteries, leveraging the abundance and low cost of Na- or K-ion.

Moreover, the material cost of these SEs can be effectively reduced. This reduction in cost could significantly impact the overall affordability of energy storage solutions. Additionally, the relatively low true density of these ionic COFs (1.6 g cm^{-3} for i-COF-1 (Na) and 1.7 g cm^{-3} for i-COF-1 (K)) offers further advantages, particularly when combined with low-cost organic electrodes that possess soft properties. This synergy could lead to the development of even more cost-effective battery systems.

Looking forward, the potential for scaling up the fabrication of freestanding SEs and optimizing the manufacturing process of COFs for large-scale applications presents an exciting avenue for practical implementation. This work not only highlights the technical merits of sulfonated ionic COFs in energy storage applications but also underscores the importance of developing sustainable, high-performance materials that can be produced economically and at scale.

■ ASSOCIATED CONTENT

Supporting Information

The Supporting Information is available free of charge at https://pubs.acs.org/doi/10.1021/acsaem.4c02760.

PXRD data; solid-state 23Na NMR; pore size distribution profile; TGA data; ion conductivity data of COF samples with various thickness or pressure; SEM image; EIS plots of without sulfonated COF, i-COF with PEO or after ball-milling; solubilities (PDF)

■ AUTHOR INFORMATION

Corresponding Author

Dawei Feng − *Department of Materials Science and Engineering, University of Wisconsin − Madison, Madison, Wisconsin 53706, United States; Department of Chemistry, University of Wisconsin − Madison, Madison, Wisconsin 53706, United States;* orcid.org/0000-0002-6285-850X; Phone: +1-6082632703; Email: dfeng23@wisc.edu

Authors

Wonmi Lee − *Department of Materials Science and Engineering, University of Wisconsin − Madison, Madison, Wisconsin 53706, United States*

Haochen Li − *Department of Materials Science and Engineering, University of Wisconsin − Madison, Madison, Wisconsin 53706, United States*

Diprajit Biswas − *Department of Mechanical Engineering, University of Wisconsin − Madison, Madison, Wisconsin 53706, United States;* orcid.org/0000-0002-4510-8168

Zhilin Du − *Department of Materials Science and Engineering, University of Wisconsin − Madison, Madison, Wisconsin 53706, United States*

Wen Ren − *Department of Electrical and Computer Engineering and Texas Center for Superconductivity at the University of Houston, University of Houston, Houston, Texas 77204, United States;* orcid.org/0000-0002-1461-6717

Lihong Zhao − *Department of Electrical and Computer Engineering and Texas Center for Superconductivity at the University of Houston, University of Houston, Houston, Texas 77204, United States;* orcid.org/0000-0003-2308-1053

Md Sariful Sheikh − *Department of Materials Science and Engineering, University of Wisconsin − Madison, Madison, Wisconsin 53706, United States*

Gyohun Choi − *Department of Materials Science and Engineering, University of Wisconsin − Madison, Madison, Wisconsin 53706, United States*

Bu Wang − *Department of Materials Science and Engineering, University of Wisconsin − Madison, Madison, Wisconsin 53706, United States; Department of Civil and Environmental Engineering, University of Wisconsin − Madison, Madison, Wisconsin 53706, United States;* orcid.org/0000-0002-9294-0918

Yan Yao − *Department of Electrical and Computer Engineering and Texas Center for Superconductivity at the University of Houston, University of Houston, Houston, Texas 77204, United States*

Eric Kazyak − *Department of Mechanical Engineering, University of Wisconsin − Madison, Madison, Wisconsin 53706, United States*

Complete contact information is available at: https://pubs.acs.org/10.1021/acsaem.4c02760

Notes

The authors declare no competing financial interest.

■ ACKNOWLEDGMENTS

This work was supported by the National Science Foundation through the EFRI program (Grant No. 2132022) and the CAREER program (Grant No. 2143569).

■ REFERENCES

(1) Ye, T.; Li, L.; Zhang, Y. Recent progress in solid electrolytes for energy storage devices. *Adv. Funct. Mater.* **2020**, *30* (29), 2000077.

(2) Manthiram, A.; Yu, X.; Wang, S. Lithium battery chemistries enabled by solid-state electrolytes. *Nat. Rev. Mater.* **2017**, *2* (4), 16103.

(3) Balaish, M.; Gonzalez-Rosillo, J. C.; Kim, K. J.; Zhu, Y.; Hood, Z. D.; Rupp, J. L. Processing thin but robust electrolytes for solid-state batteries. *Nat. Energy* **2021**, *6* (3), 227−239.

(4) Schlautmann, E.; Weiß, A.; Maus, O.; Ketter, L.; Rana, M.; Puls, S.; Nickel, V.; Gabbey, C.; Hartnig, C.; Bielefeld, A.; Zeier, W. G. Impact of the Solid Electrolyte Particle Size Distribution in Sulfide-Based Solid-State Battery Composites. *Adv. Energy Mater.* **2023**, *13* (41), 2302309.

(5) Chen, R.; Li, Q.; Yu, X.; Chen, L.; Li, H. Approaching practically accessible solid-state batteries: stability issues related to solid electrolytes and interfaces. *Chem. Rev.* **2020**, *120* (14), 6820−6877.

(6) Yu, C.; Ganapathy, S.; Van Eck, E. R. H.; Wang, H.; Basak, S.; Li, Z.; Wagemaker, M. Accessing the bottleneck in all-solid state batteries, lithium-ion transport over the solid-electrolyte-electrode interface. *Nat. Commun.* **2017**, *8* (1), 1086.

(7) Feng, X.; Fang, H.; Wu, N.; Liu, P.; Jena, P.; Nanda, J.; Mitlin, D. Review of modification strategies in emerging inorganic solid-state electrolytes for lithium, sodium, and potassium batteries. *Joule* **2022**, *6* (3), 543−587.

(8) Dong, Y.; Wen, P.; Shi, H.; Yu, Y.; Wu, Z.-S. Solid-State Electrolytes for Sodium Metal Batteries: Recent Status and Future Opportunities. *Adv. Energy Mater.* **2024**, *34* (5), 2213584.

(9) Zhang, X.; Meng, J.; Wang, X.; Xiao, Z.; Wu, P.; Mai, L. Comprehensive insights into electrolytes and solid electrolyte interfaces in potassium-ion batteries. *Energy Storage Mater.* **2021**, *38*, 30−49.

(10) Kang, L.; Liu, S.; Zhang, Q.; Zou, J.; Ai, J.; Qiao, D.; Zhong, W.; Liu, Y.; Jun, S. C.; Yamauchi, Y.; Zhang, J. Hierarchical spatial confinement unlocking the storage limit of MoS2 for flexible high-energy supercapacitors. *ACS Nano* **2024**, *18* (3), 2149−2161.

(11) Liu, S.; Kang, L.; Jun, S. C. Challenges and strategies toward cathode materials for rechargeable potassium-ion batteries. *Adv. Mater.* **2021**, *33* (47), 2004689.

(12) Liu, S.; Kang, L.; Henzie, J.; Zhang, J.; Ha, J.; Amin, M. A.; Hossain, M. S. A.; Jun, S. C.; Yamauchi, Y. Recent advances and perspectives of battery-type anode materials for potassium ion storage. *ACS Nano* **2021**, *15* (12), 18931−18973.

(13) Duan, L.; Zhang, Y.; Tang, H.; Liao, J.; Zhou, G.; Zhou, X. Recent Advances in High-Entropy Layered Oxide Cathode Materials for Alkali Metal-Ion Batteries. *Adv. Mater.* **2024**, 2411426.

(14) Xu, Y.; Du, Y.; Chen, H.; Chen, J.; Ding, T.; Sun, D.; Kim, D. H.; Lin, Z.; Zhou, X. Recent advances in rational design for high-performance potassium-ion batteries. *Chem. Soc. Rev.* **2024**, *53*, 7202−7298.

(15) Sun, J.; Kang, F.; Yan, D.; Ding, T.; Wang, Y.; Zhou, X.; Zhang, Q. Recent Progress in Using Covalent Organic Frameworks to Stabilize Metal Anodes for Highly-Efficient Rechargeable Batteries. *Angew. Chem. Int. Ed.* **2024**, *63*, No. e202406511.

(16) Xu, T.; Sun, W.; Kong, T.; Zhou, J.; Qian, Y. Stable Graphite Interface for Potassium Ion Battery Achieving Ultralong Cycling Performance. *Acta Phys. -Chim. Sin.* **2024**, *40*, 2303021.

(17) Sun, J.; Fei, Y.; Tang, H.; Bao, J.; Zhang, Q.; Zhou, X. Covalent organic frameworks as promising electrode materials for high-valent ion rechargeable batteries. *ACS Appl. Energy Mater.* **2024**, *7* (18), 7592−7602.

(18) Sun, J.; Xu, Y.; Lv, Y.; Zhang, Q.; Zhou, X. Recent advances in covalent organic framework electrode materials for alkali metal-ion batteries. *CCS Chem.* **2023**, *5* (6), 1259−1276.

(19) Famprikis, T.; Canepa, P.; Dawson, J. A.; Islam, M. S.; Masquelier, C. Fundamentals of inorganic solid-state electrolytes for batteries. *Nat. Mater.* **2019**, *18* (12), 1278−1291.

(20) Wu, F.; Zhang, K.; Liu, Y.; Gao, H.; Bai, Y.; Wang, X.; Wu, C. Polymer electrolytes and interfaces toward solid-state batteries: Recent advances and prospects. *Energy Storage Mater.* **2020**, *33*, 26−54.

(21) Bhanja, P.; Palui, A.; Chatterjee, S.; Kaneti, Y. V.; Na, J.; Sugahara, Y.; Bhaumik, A.; Yamauchi, Y. Crystalline porous organic polymer bearing− SO_3H functionality for high proton conductivity. *ACS Sustainable Chem. Eng.* **2020**, *8* (6), 2423−2432.

(22) Lei, Z.; Wayment, L. J.; Cahn, J. R.; Chen, H.; Huang, S.; Wang, X.; Jin, Y.; Sharma, S.; Zhang, W. Cyanurate-Linked Covalent Organic Frameworks Enabled by Dynamic Nucleophilic Aromatic Substitution. *J. Am. Chem. Soc.* **2022**, *144* (39), 17737−17742.

(23) Lu, F.; Gao, Y. Covalent Organic Frameworks for Ion Conduction. In Covalent Organic Frameworks. *IntechOpen* **2022**.

(24) Zhang, H.; Geng, Y.; Huang, J.; Wang, Z.; Du, K.; Li, H. Charge and mass transport mechanisms in two-dimensional covalent organic frameworks (2D COFs) for electrochemical energy storage devices. *Energy Environ. Sci.* **2023**, *16* (3), 889−951.

(25) Lee, W.; Li, H.; Du, Z.; Feng, D. Ion transport mechanisms in covalent organic frameworks: implications for technology. *Chem. Soc. Rev.* **2024**, *53*, 8182−8201.

(26) Jeong, K.; Park, S.; Jung, G. Y.; Kim, S. H.; Lee, Y. H.; Kwak, S. K.; Lee, S. Y. Solvent-free, single lithium-ion conducting covalent organic frameworks. *J. Am. Chem. Soc.* **2019**, *141* (14), 5880−5885.

(27) Chen, L.; Li, W.; Fan, L.-Z.; Nan, C.-W.; Zhang, Q. Intercalated electrolyte with high transference number for dendrite-free solid-state lithium batteries. *Adv. Funct. Mater.* **2019**, *29* (28), 1901047.

(28) Zhang, J.; Luo, D.; Xiao, H.; Zhao, H.; Ding, B.; Dou, H.; Zhang, X. Post-synthetic covalent organic framework to improve the performance of solid-state Li^+ electrolytes. *ACS Appl. Mater. Interfaces* **2023**, *15* (29), 34704−34710.

(29) Shan, Z.; Wu, M.; Du, Y.; Xu, B.; He, B.; Wu, X.; Zhang, G. Covalent organic framework-based electrolytes for fast Li^+ conduction and high-temperature solid-state lithium-ion batteries. *Chem. Mater.* **2021**, *33* (13), 5058−5066.

(30) Zhang, K.; Zhang, B.; Weng, M.; Zheng, J.; Li, S.; Pan, F. Lithium ion diffusion mechanism in covalent organic framework based solid state electrolyte. *Phys. Chem. Chem. Phys.* **2019**, *21*, 9883−9888.

(31) Fernando, I. R.; Daskalakis, N.; Demadis, K. D.; Mezei, G. Cation effect on the inorganic−organic layered structure of pyrazole-

4-sulfonate networks and inhibitory effects on copper corrosion. *New J. Chem.* **2010**, *34* (2), 221−235.
(32) Zhu, L.; Wang, Y.; Chen, J.; Li, W.; Wang, T.; Wu, J.; Han, S.; Xia, Y.; Wu, Y.; Wu, M.; Wang, F.; Zheng, Y.; Peng, L.; Liu, J.; Chen, L.; Tang, W. Enhancing ionic conductivity in solid electrolyte by relocating diffusion ions to under-coordination sites. *Sci. Adv.* **2022**, *8* (11), No. eabj7698.
(33) Vadhva, P.; Hu, J.; Johnson, M. J.; Stocker, R.; Braglia, M.; Brett, D. J.; Rettie, A. J. Electrochemical impedance spectroscopy for all-solid-state batteries: theory, methods and future outlook. *ChemElectrochem* **2021**, *8* (11), 1930−1947.
(34) Liu, S.; Kang, L.; Zhang, J.; Jun, S. C.; Yamauchi, Y. Carbonaceous anode materials for non-aqueous sodium-and potassium-ion hybrid capacitors. *ACS Energy Lett.* **2021**, *6* (11), 4127−4154.
(35) Zhao, G.; Xu, L.; Jiang, J.; Mei, Z.; An, Q.; Lv, P.; Yang, X.; Guo, H.; Sun, X. COFs-based electrolyte accelerates the Na^+ diffusion and restrains dendrite growth in quasi-solid-state organic batteries. *Nano Energy* **2022**, *92*, 106756.
(36) Yan, Y.; Liu, Z.; Wan, T.; Li, W.; Qiu, Z.; Chi, C.; Huangfu, C.; Wang, G.; Qi, B.; Yan, Y.; Wei, T.; Fan, Z. Bioinspired design of Na-ion conduction channels in covalent organic frameworks for quasi-solid-state sodium batteries. *Nat. Commun.* **2023**, *14* (1), 3066.
(37) Zettl, R.; Lunghammer, S.; Gadermaier, B.; Boulaoued, A.; Johansson, P.; Wilkening, H. M. R.; Hanzu, I. High Li^+ and Na^+ Conductivity in New Hybrid Solid Electrolytes Based on the Porous MIL-121 Metal Organic Framework. *Adv. Energy Mater.* **2021**, *11* (16), 2003542.
(38) Yu, X.; Grundish, N.; Goodenough, J.; Manthiram, A. Ionic Liquid (IL) Laden Metal−Organic Framework (IL-MOF) Electrolyte for Quasi-Solid-State Sodium Batteries. *ACS Appl. Mater. Interfaces* **2021**, *13* (21), 24662−24669.
(39) Zhang, Z.; Huang, Y.; Li, C.; Li, X. Metal−Organic Framework-Supported Poly(ethylene oxide) Composite Gel Polymer Electrolytes for High-Performance Lithium/Sodium Metal Batteries. *ACS Appl. Mater. Interfaces* **2021**, *13* (31), 37262−37272.
(40) Zhou, B.; Le, J.; Cheng, Z.; Zhao, X.; Shen, M.; Xie, M.; Hu, B.; Yang, X.; Chen, L.; Chen, H. Simple Transformation of Covalent Organic Frameworks to Highly Proton-Conductive Electrolytes. *ACS Appl. Mater. Interfaces* **2020**, *12* (7), 8198−8205.
(41) Gu, Y. J.; Lo, Y. A.; Li, A. C.; Chen, Y. C.; Li, J. H.; Wang, Y. S.; Tian, H. K.; Kaveevivitchai, W.; Kung, C. W. A Single Potassium-Ion Conducting Metal−Organic Framework. *ACS Appl. Energy Mater.* **2022**, *5* (7), 8573−8580.
(42) Jeong, K.; Park, S.; Jung, G.; Kim, S.; Lee, Y.; Kwak, S.; Lee, S. Solvent-Free, Single Lithium-Ion Conducting Covalent Organic Frameworks. *J. Am. Chem. Soc.* **2019**, *141* (14), 5880−5885.
(43) Wu, J.; Guo, X. MOF-derived nanoporous multifunctional fillers enhancing the performances of polymer electrolytes for solid-state lithium batteries. *J. Mater. Chem. A* **2019**, *7* (6), 2653−2659.
(44) Li, Z.; Liu, Z.-W.; Li, Z.; Wang, T.-X.; Zhao, F.; Ding, X.; Feng, W.; Han, B.-H. Defective 2D covalent organic frameworks for postfunctionalization. *Adv. Funct. Mater.* **2020**, *30* (10), 1909267.
(45) Hu, Y.; Dunlap, N.; Wan, S.; Lu, S.; Huang, S.; Sellinger, I.; Ortiz, M.; Jin, Y.; Lee, S.-H.; Zhang, W. Crystalline lithium imidazolate covalent organic frameworks with high Li-ion conductivity. *J. Mater. Chem. A* **2019**, *141* (18), 7518−7525.
(46) Li, X.; Tian, Y.; Shen, L.; Qu, Z.; Ma, T.; Sun, F.; Liu, X.; Zhang, C.; Shen, J.; Li, X.; Gao, L.; et al. Electrolyte interphase built from anionic covalent organic frameworks for lithium dendrite suppression. *Adv. Funct. Mater.* **2021**, *31* (22), 2009718.
(47) Hayashi, A.; Noi, K.; Sakuda, A.; Tatsumisago, M. Superionic glass-ceramic electrolytes for room-temperature rechargeable sodium batteries. *Nat. Commun.* **2012**, *3* (1), 856.
(48) Li, X.; Cai, S.; Sun, B.; Yang, C.; Zhang, J.; Liu, Y. Chemically robust covalent organic frameworks: progress and perspective. *Matter* **2020**, *3* (5), 1507−1540.
(49) Guin, M.; Tietz, F.; Guillon, O. New promising NASICON material as solid electrolyte for sodium-ion batteries: Correlation between composition, crystal structure and ionic conductivity of $Na_{3+x}Sc_2Si_xP_{3-x}O_{12}$. *Solid State Ionics* **2016**, *293*, 18−26.
(50) Sun, F.; Xiang, Y.; Sun, Q.; Zhong, G.; Banis, M. N.; Liu, Y.; Li, R.; Fu, R.; Zheng, M.; Sham, T.-K.; Yang, Y.; Sun, X.; Sun, X. Origin of high ionic conductivity of Sc-doped sodium-rich NASICON solid-state electrolytes. *Adv. Funct. Mater.* **2021**, *31* (31), 2102129.
(51) Chong, M. K.; Zainuddin, Z.; Omar, F. S.; Jumali, M. H. H. $Na_3Zr_2(SiO_4)_2PO_4$ NASICON-type solid electrolyte: influence of milling duration on microstructure and ionic conductivity mechanism. *Ceram. Int.* **2022**, *48* (15), 22106−22113.
(52) Liu, L.; Ma, Q.; Zhou, X.; Ding, Z.; Grüner, D.; Kübel, C.; Tietz, F. Simultaneously improving sodium ionic conductivity and dendrite behavior of NaSICON ceramics by grain-boundary modification. *J. Power Sources* **2025**, *626*, 235773.
(53) Guan, S.; Lu, J.; Li, Y.; Xie, D.; Zhuang, C.; Zhang, W. Influence of calcium-doped on the conductivity of NASICON-type Na3Zr2Si2PO4 solid electrolyte. *Ceram. Int.* **2024**.
(54) Hayashi, A.; Noi, K.; Tanibata, N.; Nagao, M.; Tatsumisago, M. High sodium ion conductivity of glass−ceramic electrolytes with cubic Na_3PS_4. *J. Power Sources* **2014**, *258*, 420−423.
(55) Sun, F.; Xiang, Y.; Sun, Q.; Zhong, G.; Banis, M. N.; Li, W.; Liu, Y.; Luo, J.; Li, R.; Fu, R.; Sham, T. K.; Yang, Y.; Sun, X.; Sun, X. Insight into Ion Diffusion Dynamics/Mechanisms and Electronic Structure of Highly Conductive Sodium-Rich $Na_{3+x}La_xZr_2-_xSi_2PO^{12}$. (0≤ x≤ 0.5) Solid-State Electrolytes. *ACS Appl. Mater. Interfaces* **2021**, *13* (11), 13132−13138.
(56) Wenzel, S.; Leichtweiss, T.; Weber, D. A.; Sann, J.; Zeier, W. G.; Janek, J. Interfacial reactivity benchmarking of the sodium ion conductors Na_3PS_4 and sodium β-alumina for protected sodium metal anodes and sodium all-solid-state batteries. *ACS Appl. Mater. Interfaces* **2016**, *8* (41), 28216−28224.
(57) Li, Y.; Wang, Q.; Zhao, X.; He, B.; Xiao, Y.; Guo, J.; Yang, L.; Liao, R. High ionic conductive Sodium β-alumina (SBA) and SBA-NaPF6 composite solid electrolytes prepared by cold sintering process. *Ceram. Int.* **2024**.
(58) Li, X.; Xu, Y.; Zhao, C.; Wu, D.; Wang, L.; Zheng, M.; Han, X.; Zhang, S.; Yue, J.; Xiao, B.; Xiao, W.; Wang, L.; Mei, T.; Gu, M.; Liang, J.; Sun, X. The Universal Super Cation-Conductivity in Multiple-cation Mixed Chloride Solid-State Electrolytes. *Angew. Chem., Int. Ed.* **2023**, *62* (48), No. e202306433.
(59) Gilardi, E.; Materzanini, G.; Kahle, L.; Dobeli, M.; Lacey, S.; Cheng, X.; Marzari, N.; Pergolesi, D.; Hintennach, A.; Lippert, T. Li4−x Ge1−x P x O4, a Potential Solid-State Electrolyte for All-Oxide Microbatteries. *ACS Appl. Energy Mater.* **2020**, *3* (10), 9910−9917.
(60) Liang, J.; Chen, N.; Li, X.; Li, X.; Adair, K. R.; Li, J.; Wang, C.; Yu, C.; Norouzi Banis, M.; Zhang, L.; Zhao, S. Li 10 Ge(P 1− x Sb x) 2 S 12 Lithium-Ion Conductors with Enhanced Atmospheric Stability. *Chem. Mater.* **2020**, *32* (6), 2664−2672.
(61) Park, K. H.; Kaup, K.; Assoud, A.; Zhang, Q.; Wu, X.; Nazar, L. F. High-voltage superionic halide solid electrolytes for all-solid-state Li-ion batteries. *ACS Energy Lett.* **2020**, *5* (2), 533−539.
(62) Inagaki, M.; Suzuki, K.; Hori, S.; Yoshino, K.; Matsui, N.; Yonemura, M.; Hirayama, M.; Kanno, R. Conduction mechanism of Li10GeP2S12-type lithium superionic conductors in a Li−Sn−Si−P−S system. *Chem. Mater.* **2019**, *31* (9), 3485−3490.
(63) Iwasaki, R.; Hori, S.; Kanno, R.; Yajima, T.; Hirai, D.; Kato, Y.; Hiroi, Z. Weak anisotropic lithium-ion conductivity in single crystals of Li10GeP2S12. *Chem. Mater.* **2019**, *31* (10), 3694−3699.

https://doi.org/10.1021/acsaem.4c02760
ACS Appl. Energy Mater. 2025, 8, 569−580